PHYSICAL REVIEW D **88,** 072009 (2013)

Measurement of the $e^+e^- \to p\bar{p}$ cross section in the energy range from 3.0 to 6.5 GeV

J. P. Lees,[1] V. Poireau,[1] V. Tisserand,[1] E. Grauges,[2] A. Palano,[3] G. Eigen,[4] B. Stugu,[4] D. N. Brown,[5] L. T. Kerth,[5] Yu. G. Kolomensky,[5] M. J. Lee,[5] G. Lynch,[5] H. Koch,[6] T. Schroeder,[6] C. Hearty,[7] T. S. Mattison,[7] J. A. McKenna,[7] R. Y. So,[7] A. Khan,[8] V. E. Blinov,[9a,9c] A. R. Buzykaev,[9a] V. P. Druzhinin,[9a,9b] V. B. Golubev,[9a,9b] E. A. Kravchenko,[9a,9b] A. P. Onuchin,[9a,9c] S. I. Serednyakov,[9a,9b] Yu. I. Skovpen,[9a,9b] E. P. Solodov,[9a,9b] K. Yu. Todyshev,[9a,9b] A. N. Yushkov,[9a] D. Kirkby,[10] A. J. Lankford,[10] M. Mandelkern,[10] B. Dey,[11] J. W. Gary,[11] O. Long,[11] G. M. Vitug,[11] C. Campagnari,[12] M. Franco Sevilla,[12] T. M. Hong,[12] D. Kovalskyi,[12] J. D. Richman,[12] C. A. West,[12] A. M. Eisner,[13] W. S. Lockman,[13] B. A. Schumm,[13] A. Seiden,[13] D. S. Chao,[14] C. H. Cheng,[14] B. Echenard,[14] K. T. Flood,[14] D. G. Hitlin,[14] P. Ongmongkolkul,[14] F. C. Porter,[14] R. Andreassen,[15] Z. Huard,[15] B. T. Meadows,[15] B. G. Pushpawela,[15] M. D. Sokoloff,[15] L. Sun,[15] P. C. Bloom,[16] W. T. Ford,[16] A. Gaz,[16] U. Nauenberg,[16] J. G. Smith,[16] S. R. Wagner,[16] R. Ayad,[17,*] W. H. Toki,[17] B. Spaan,[18] R. Schwierz,[19] D. Bernard,[20] M. Verderi,[20] S. Playfer,[21] D. Bettoni,[22a] C. Bozzi,[22a] R. Calabrese,[22a,22b] G. Cibinetto,[22a,22b] E. Fioravanti,[22a,22b] I. Garzia,[22a,22b] E. Luppi,[22a,22b] L. Piemontese,[22a] V. Santoro,[22a] R. Baldini-Ferroli,[23] A. Calcaterra,[23] R. de Sangro,[23] G. Finocchiaro,[23] S. Martellotti,[23] P. Patteri,[23] I. M. Peruzzi,[23,†] M. Piccolo,[23] M. Rama,[23] A. Zallo,[23] R. Contri,[24a,24b] E. Guido,[24a,24b] M. Lo Vetere,[24a,24b] M. R. Monge,[24a,24b] S. Passaggio,[24a] C. Patrignani,[24a,24b] E. Robutti,[24a] B. Bhuyan,[25] V. Prasad,[25] M. Morii,[26] A. Adametz,[27] U. Uwer,[27] H. M. Lacker,[28] P. D. Dauncey,[29] U. Mallik,[30] C. Chen,[31] J. Cochran,[31] W. T. Meyer,[31] S. Prell,[31] A. V. Gritsan,[32] N. Arnaud,[33] M. Davier,[33] D. Derkach,[33] G. Grosdidier,[33] F. Le Diberder,[33] A. M. Lutz,[33] B. Malaescu,[33,‡] P. Roudeau,[33] A. Stocchi,[33] G. Wormser,[33] D. J. Lange,[34] D. M. Wright,[34] J. P. Coleman,[35] J. R. Fry,[35] E. Gabathuler,[35] D. E. Hutchcroft,[35] D. J. Payne,[35] C. Touramanis,[35] A. J. Bevan,[36] F. Di Lodovico,[36] R. Sacco,[36] G. Cowan,[37] J. Bougher,[38] D. N. Brown,[38] C. L. Davis,[36] A. G. Denig,[39] M. Fritsch,[39] W. Gradl,[39] K. Griessinger,[39] A. Hafner,[39] E. Prencipe,[39] K. R. Schubert,[39] R. J. Barlow,[40,§] G. D. Lafferty,[40] E. Behn,[41] R. Cenci,[41] B. Hamilton,[41] A. Jawahery,[41] D. A. Roberts,[41] R. Cowan,[42] D. Dujmic,[42] G. Sciolla,[42] R. Cheaib,[43] P. M. Patel,[43,‖] S. H. Robertson,[43] P. Biassoni,[44a,44b] N. Neri,[44a] F. Palombo,[44a,44b] L. Cremaldi,[45] R. Godang,[45,¶] P. Sonnek,[45] D. J. Summers,[45] M. Simard,[46] P. Taras,[46] G. De Nardo,[47] D. Monorchio,[47] G. Onorato,[47] C. Sciacca,[47] M. Martinelli,[48] G. Raven,[48] C. P. Jessop,[49] J. M. LoSecco,[49] K. Honscheid,[50] R. Kass,[50] J. Brau,[51] R. Frey,[51] N. B. Sinev,[51] D. Strom,[51] E. Torrence,[51] E. Feltresi,[52a,52b] M. Margoni,[52a,52b] M. Morandin,[52a] M. Posocco,[52a] M. Rotondo,[52a] G. Simi,[52a] F. Simonetto,[52a,52b] R. Stroili,[52a,52b] S. Akar,[53] E. Ben-Haim,[53] M. Bomben,[53] G. R. Bonneaud,[53] H. Briand,[53] G. Calderini,[53] J. Chauveau,[53] Ph. Leruste,[53] G. Marchiori,[53] J. Ocariz,[53] S. Sitt,[53] M. Biasini,[54a,54b] E. Manoni,[54a] S. Pacetti,[54a,54b] A. Rossi,[54a] C. Angelini,[55a,55b] G. Batignani,[55a,55b] S. Bettarini,[55a,55b] M. Carpinelli,[55a,55b,**] G. Casarosa,[55a,55b] A. Cervelli,[55a,55b] F. Forti,[55a,55b] M. A. Giorgi,[55a,55b] A. Lusiani,[55a,55c] B. Oberhof,[55a,55b] E. Paoloni,[55a,55b] A. Perez,[54a] G. Rizzo,[55a,55b] J. J. Walsh,[55a] D. Lopes Pegna,[56] J. Olsen,[56] A. J. S. Smith,[56] R. Faccini,[57a,57b] F. Ferrarotto,[57a] F. Ferroni,[57a,57b] M. Gaspero,[57a,57b] L. Li Gioi,[57a] G. Piredda,[57a] C. Bünger,[58] O. Grünberg,[58] T. Hartmann,[58] T. Leddig,[58] C. Voß,[58] R. Waldi,[58] T. Adye,[59] E. O. Olaiya,[59] F. F. Wilson,[59] S. Emery,[60] G. Hamel de Monchenault,[60] G. Vasseur,[60] Ch. Yèche,[60] F. Anulli,[61,††] D. Aston,[61] D. J. Bard,[61] J. F. Benitez,[61] C. Cartaro,[61] M. R. Convery,[61] J. Dorfan,[61] G. P. Dubois-Felsmann,[61] W. Dunwoodie,[61] M. Ebert,[61] R. C. Field,[61] B. G. Fulsom,[61] A. M. Gabareen,[61] M. T. Graham,[61] C. Hast,[61] W. R. Innes,[61] P. Kim,[61] M. L. Kocian,[61] D. W. G. S. Leith,[61] P. Lewis,[61] D. Lindemann,[61] B. Lindquist,[61] S. Luitz,[61] V. Luth,[61] H. L. Lynch,[61] D. B. MacFarlane,[61] D. R. Muller,[61] H. Neal,[61] S. Nelson,[61] M. Perl,[61] T. Pulliam,[61] B. N. Ratcliff,[61] A. Roodman,[61] A. A. Salnikov,[61] R. H. Schindler,[61] A. Snyder,[61] D. Su,[61] M. K. Sullivan,[61] J. Va'vra,[61] A. P. Wagner,[61] W. F. Wang,[61] W. J. Wisniewski,[61] M. Wittgen,[61] D. H. Wright,[61] H. W. Wulsin,[61] V. Ziegler,[61] W. Park,[62] M. V. Purohit,[62] R. M. White,[62,‡‡] J. R. Wilson,[62] A. Randle-Conde,[63] S. J. Sekula,[63] M. Bellis,[64] P. R. Burchat,[64] T. S. Miyashita,[64] E. M. T. Puccio,[64] M. S. Alam,[65] J. A. Ernst,[65] R. Gorodeisky,[66] N. Guttman,[66] D. R. Peimer,[66] A. Soffer,[66] S. M. Spanier,[67] J. L. Ritchie,[68] A. M. Ruland,[68] R. F. Schwitters,[68] B. C. Wray,[68] J. M. Izen,[69] X. C. Lou,[69] F. Bianchi,[70a,70b] F. De Mori,[70a,70b] A. Filippi,[70a] D. Gamba,[70a,70b] S. Zambito,[70a,70b] L. Lanceri,[71a,71b] L. Vitale,[71a,71b] F. Martinez-Vidal,[72] A. Oyanguren,[72] P. Villanueva-Perez,[72] H. Ahmed,[73] J. Albert,[73] Sw. Banerjee,[73] F. U. Bernlochner,[73] H. H. F. Choi,[73] G. J. King,[73] R. Kowalewski,[73] M. J. Lewczuk,[73] T. Lueck,[73] I. M. Nugent,[73] J. M. Roney,[73] R. J. Sobie,[73] N. Tasneem,[73] T. J. Gershon,[74] P. F. Harrison,[74] T. E. Latham,[74] H. R. Band,[75] S. Dasu,[75] Y. Pan,[75] R. Prepost,[75] and S. L. Wu[75]

(*BABAR* Collaboration)

[1]*Laboratoire d'Annecy-le-Vieux de Physique des Particules (LAPP), Université de Savoie, CNRS/IN2P3, F-74941 Annecy-Le-Vieux, France*
[2]*Universitat de Barcelona, Facultat de Fisica, Departament ECM, E-08028 Barcelona, Spain*
[3]*INFN Sezione di Bari, I-70125 Bari, Italy and Dipartimento di Fisica, Università di Bari, I-70126 Bari, Italy*
[4]*University of Bergen, Institute of Physics, N-5007 Bergen, Norway*
[5]*Lawrence Berkeley National Laboratory and University of California, Berkeley, California 94720, USA*
[6]*Ruhr Universität Bochum, Institut für Experimentalphysik 1, D-44780 Bochum, Germany*
[7]*University of British Columbia, Vancouver, British Columbia V6T 1Z1, Canada*
[8]*Brunel University, Uxbridge, Middlesex UB8 3PH, United Kingdom*
[9a]*Budker Institute of Nuclear Physics SB RAS, Novosibirsk 630090, Russia*
[9b]*Novosibirsk State University, Novosibirsk 630090, Russia*
[9c]*Novosibirsk State Technical University, Novosibirsk 630092, Russia*
[10]*University of California at Irvine, Irvine, California 92697, USA*
[11]*University of California at Riverside, Riverside, California 92521, USA*
[12]*University of California at Santa Barbara, Santa Barbara, California 93106, USA*
[13]*University of California at Santa Cruz, Institute for Particle Physics, Santa Cruz, California 95064, USA*
[14]*California Institute of Technology, Pasadena, California 91125, USA*
[15]*University of Cincinnati, Cincinnati, Ohio 45221, USA*
[16]*University of Colorado, Boulder, Colorado 80309, USA*
[17]*Colorado State University, Fort Collins, Colorado 80523, USA*
[18]*Technische Universität Dortmund, Fakultät Physik, D-44221 Dortmund, Germany*
[19]*Technische Universität Dresden, Institut für Kern- und Teilchenphysik, D-01062 Dresden, Germany*
[20]*Laboratoire Leprince-Ringuet, Ecole Polytechnique, CNRS/IN2P3, F-91128 Palaiseau, France*
[21]*University of Edinburgh, Edinburgh EH9 3JZ, United Kingdom*
[22a]*INFN Sezione di Ferrara, I-44122 Ferrara, Italy*
[22b]*Dipartimento di Fisica e Scienze della Terra, Università di Ferrara, I-44122 Ferrara, Italy*
[23]*INFN Laboratori Nazionali di Frascati, I-00044 Frascati, Italy*
[24a]*INFN Sezione di Genova, I-16146 Genova, Italy*
[24b]*Dipartimento di Fisica, Università di Genova, I-16146 Genova, Italy*
[25]*Indian Institute of Technology Guwahati, Guwahati, Assam, 781 039, India*
[26]*Harvard University, Cambridge, Massachusetts 02138, USA*
[27]*Universität Heidelberg, Physikalisches Institut, D-69120 Heidelberg, Germany*
[28]*Humboldt-Universität zu Berlin, Institut für Physik, D-12489 Berlin, Germany*
[29]*Imperial College London, London SW7 2AZ, United Kingdom*
[30]*University of Iowa, Iowa City, Iowa 52242, USA*
[31]*Iowa State University, Ames, Iowa 50011-3160, USA*
[32]*Johns Hopkins University, Baltimore, Maryland 21218, USA*
[33]*Laboratoire de l'Accélérateur Linéaire, IN2P3/CNRS et Université Paris-Sud 11, Centre Scientifique d'Orsay, F-91898 Orsay Cedex, France*
[34]*Lawrence Livermore National Laboratory, Livermore, California 94550, USA*
[35]*University of Liverpool, Liverpool L69 7ZE, United Kingdom*
[36]*Queen Mary, University of London, London E1 4NS, United Kingdom*
[37]*University of London, Royal Holloway and Bedford New College, Egham, Surrey TW20 0EX, United Kingdom*
[38]*University of Louisville, Louisville, Kentucky 40292, USA*
[39]*Johannes Gutenberg-Universität Mainz, Institut für Kernphysik, D-55099 Mainz, Germany*
[40]*University of Manchester, Manchester M13 9PL, United Kingdom*
[41]*University of Maryland, College Park, Maryland 20742, USA*
[42]*Massachusetts Institute of Technology, Laboratory for Nuclear Science, Cambridge, Massachusetts 02139, USA*
[43]*McGill University, Montréal, Québec H3A 2T8, Canada*
[44a]*INFN Sezione di Milano, I-20133 Milano, Italy*
[44b]*Dipartimento di Fisica, Università di Milano, I-20133 Milano, Italy*
[45]*University of Mississippi, University, Mississippi 38677, USA*
[46]*Université de Montréal, Physique des Particules, Montréal, Québec H3C 3J7, Canada*
[47]*INFN Sezione di Napoli, I-80126 Napoli, Italy and Dipartimento di Scienze Fisiche, Università di Napoli Federico II, I-80126 Napoli, Italy*
[48]*NIKHEF, National Institute for Nuclear Physics and High Energy Physics, NL-1009 DB Amsterdam, Netherlands*
[49]*University of Notre Dame, Notre Dame, Indiana 46556, USA*

[50]*Ohio State University, Columbus, Ohio 43210, USA*
[51]*University of Oregon, Eugene, Oregon 97403, USA*
[52a]*INFN Sezione di Padova, I-35131 Padova, Italy*
[52b]*Dipartimento di Fisica, Università di Padova, I-35131 Padova, Italy*
[53]*Laboratoire de Physique Nucléaire et de Hautes Energies, IN2P3/CNRS, Université Pierre et Marie Curie-Paris 6, Université Denis Diderot-Paris 7, F-75252 Paris, France*
[54a]*INFN Sezione di Perugia, I-06123 Perugia, Italy*
[54b]*Dipartimento di Fisica, Università di Perugia, I-06123 Perugia, Italy*
[55a]*INFN Sezione di Pisa, I-56127 Pisa, Italy*
[55b]*Dipartimento di Fisica, Università di Pisa, I-56126 Pisa, Italy*
[55c]*Scuola Normale Superiore di Pisa, I-56127 Pisa, Italy*
[56]*Princeton University, Princeton, New Jersey 08544, USA*
[57a]*INFN Sezione di Roma, I-00185 Roma, Italy*
[57b]*Dipartimento di Fisica, Università di Roma La Sapienza, I-00185 Roma, Italy*
[58]*Universität Rostock, D-18051 Rostock, Germany*
[59]*Rutherford Appleton Laboratory, Chilton, Didcot, Oxon OX11 0QX, United Kingdom*
[60]*CEA, Irfu, SPP, Centre de Saclay, F-91191 Gif-sur-Yvette, France*
[61]*SLAC National Accelerator Laboratory, Stanford, California 94309 USA*
[62]*University of South Carolina, Columbia, South Carolina 29208, USA*
[63]*Southern Methodist University, Dallas, Texas 75275, USA*
[64]*Stanford University, Stanford, California 94305-4060, USA*
[65]*State University of New York, Albany, New York 12222, USA*
[66]*Tel Aviv University, School of Physics and Astronomy, Tel Aviv 69978, Israel*
[67]*University of Tennessee, Knoxville, Tennessee 37996, USA*
[68]*University of Texas at Austin, Austin, Texas 78712, USA*
[69]*University of Texas at Dallas, Richardson, Texas 75083, USA*
[70a]*INFN Sezione di Torino, I-10125 Torino, Italy*
[70b]*Dipartimento di Fisica, Università di Torino, I-10125 Torino, Italy*
[71a]*INFN Sezione di Trieste, I-34127 Trieste, Italy*
[71b]*Dipartimento di Fisica, Università di Trieste, I-34127 Trieste, Italy*
[72]*IFIC, Universitat de Valencia-CSIC, E-46071 Valencia, Spain*
[73]*University of Victoria, Victoria, British Columbia V8W 3P6, Canada*
[74]*Department of Physics, University of Warwick, Coventry CV4 7AL, United Kingdom*
[75]*University of Wisconsin, Madison, Wisconsin 53706, USA*
(Received 8 August 2013; published 28 October 2013)

The $e^+e^- \to p\bar{p}$ cross section and the proton magnetic form factor have been measured in the center-of-mass energy range from 3.0 to 6.5 GeV using the initial-state radiation technique with an undetected photon. This is the first measurement of the form factor at energies higher than 4.5 GeV. The analysis is based on 469 fb^{-1} of integrated luminosity collected with the *BABAR* detector at the PEP-II collider at e^+e^- center-of-mass energies near 10.6 GeV. The branching fractions for the decays $J/\psi \to p\bar{p}$ and $\psi(2S) \to p\bar{p}$ have also been measured.

DOI: 10.1103/PhysRevD.88.072009 PACS numbers: 13.66.Bc, 14.20.Dh, 13.40.Gp, 13.25.Gv

I. INTRODUCTION

In this paper, we analyze the initial-state radiation (ISR) process $e^+e^- \to p\bar{p}\gamma$ represented by Fig. 1. This analysis is a continuation of our previous studies [1,2], where the ISR technique was used to measure the cross section of the nonradiative process $e^+e^- \to p\bar{p}$ over the center-of-mass (c.m.) energy range from the $p\bar{p}$ threshold, $2m_pc^2 = 1.88$ GeV, up to 4.5 GeV. In Refs. [1,2] it is required that the ISR photon be detected (large-angle ISR). In this paper, we analyze events in which the ISR photon is emitted along the e^+e^- collision axis (small-angle ISR) and is therefore not detected. This allows us to increase the detection efficiency for ISR events with $p\bar{p}$ invariant mass above 3.2 GeV/c^2, to select $p\bar{p}\gamma$ events

*Present address: University of Tabuk, Tabuk 71491, Saudi Arabia.
†Also at Università di Perugia, Dipartimento di Fisica, I-06123 Perugia, Italy.
‡Present address: Laboratoire de Physique Nucláire et de Hautes Energies, IN2P3/CNRS, Paris, France.
§Present address: University of Huddersfield, Huddersfield HD1 3DH, United Kingdom.
‖Deceased.
¶Present address: University of South Alabama, Mobile, Alabama 36688, USA.
**Also at Università di Sassari, I-07100 Sassari, Italy.
††Also at INFN Sezione di Roma, I-00185 Roma, Italy.
‡‡Present address: Universidad Técnica Federico Santa Maria, Valparaiso 2390123, Chile.

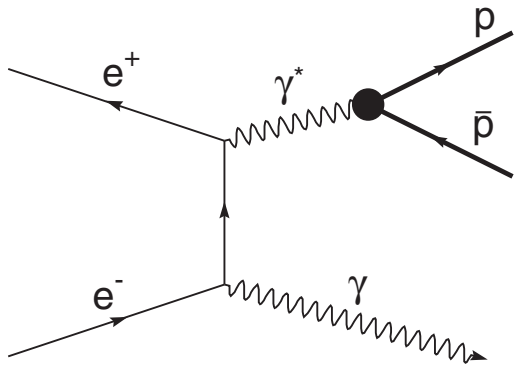

FIG. 1. The Feynman diagram for the ISR process $e^+e^- \to p\bar{p}\gamma$.

with a lower background, and, therefore, to extend the energy range for measurement of the $e^+e^- \to p\bar{p}$ cross section. A discussion of the difference between the large- and small-angle ISR techniques is given in Ref. [3].

The Born cross section for the ISR process integrated over the nucleon momenta and the photon polar angle is given by

$$\frac{\mathrm{d}\sigma_{e^+e^-\to p\bar{p}\gamma}(M_{p\bar{p}})}{\mathrm{d}M_{p\bar{p}}} = \frac{2M_{p\bar{p}}}{s} W(s,x)\sigma_{p\bar{p}}(M_{p\bar{p}}), \quad (1)$$

where $M_{p\bar{p}}$ is the $p\bar{p}$ invariant mass, s is the e^+e^- c.m. energy squared, $x \equiv E^*_\gamma/\sqrt{s} = 1 - M^2_{p\bar{p}}/s$, and E^*_γ is the ISR photon energy in the e^+e^- c.m. frame.[1] The function [3]

$$W(s,x) = \frac{\alpha}{\pi x}\left(\ln\frac{s}{m_e^2} - 1\right)(2 - 2x + x^2) \quad (2)$$

specifies the probability of ISR photon emission, where α is the fine structure constant and m_e is the electron mass. Equations (1) and (2) describe ISR processes at the lowest QED order. To calculate the function $W(x)$ more precisely, taking into account higher-order diagrams involving loops and extra photon emission, we make use of the analytic techniques described in Refs. [4–6] and the Monte Carlo (MC) generator of ISR events, PHOKHARA [7].

The cross section for $e^+e^- \to p\bar{p}$ is given by

$$\sigma_{p\bar{p}}(M_{p\bar{p}}) = \frac{4\pi\alpha^2\beta C}{3M^2_{p\bar{p}}}\left[|G_M(M_{p\bar{p}})|^2 + \frac{2m_p^2}{M^2_{p\bar{p}}}|G_E(M_{p\bar{p}})|^2\right], \quad (3)$$

where $\beta = \sqrt{1 - 4m_p^2/M^2_{p\bar{p}}}$, $C = y/(1 - e^{-y})$ is the Coulomb correction factor [8], and $y = \pi\alpha(1 + \beta^2)/\beta$. The Coulomb factor makes the cross section nonzero at threshold. The cross section depends on the magnetic (G_M) and electric (G_E) form factors. At large $p\bar{p}$ invariant masses, the second term in Eq. (3) is suppressed as $2m_p^2/M^2_{p\bar{p}}$, and therefore the measured total cross section is not very sensitive to the value of the electric form factor. The value of the magnetic form factor can be extracted from the measured cross section with relatively small model uncertainty using, for example, the assumption that $|G_M| = |G_E|$ [9–11].

The existing experimental data on $|G_M(M_{p\bar{p}})|$ at high $p\bar{p}$ invariant masses were obtained in e^+e^- [2,9–11] and $p\bar{p}$ annihilation [12,13]. At energies higher than 3 GeV, the value of the magnetic form factor decreases rapidly with increasing energy. The energy dependence measured in Refs. [2,10,12,13] agrees with the dependence $\alpha_s^2(M^2_{p\bar{p}})/M^4_{p\bar{p}}$ predicted by QCD for the asymptotic proton form factor [14]. However, the two precision measurements of Ref. [11] based on CLEO data indicate that the decrease of the form factor at energies near 4 GeV is somewhat slower.

In this work, we improve the accuracy of our measurements of the $e^+e^- \to p\bar{p}$ cross section and of the proton magnetic form factor for $p\bar{p}$ invariant masses greater than 3 GeV/c^2, and we extend the range of measurement up to 6.5 GeV/c^2.

II. THE *BABAR* DETECTOR, DATA AND SIMULATED SAMPLES

We analyze a data sample corresponding to an integrated luminosity of 469 fb^{-1} [15] recorded with the *BABAR* detector [16] at the SLAC PEP-II asymmetric energy (9 GeV e^- and 3.1 GeV e^+) collider. About 90% of the data were collected at an e^+e^- c.m. energy of 10.58 GeV [the $\Upsilon(4S)$ mass], and the remainder at 10.54 GeV.

Charged particle tracking is provided by a 5-layer silicon vertex tracker (SVT) and a 40-layer drift chamber (DCH), operating in the 1.5 T magnetic field of a superconducting solenoid. The transverse momentum resolution is 0.47% at 1 GeV/c. The position and energy of a photon-produced cluster are measured with a CsI(Tl) electromagnetic calorimeter. Charged particle identification (PID) is provided by specific ionization measurements in the SVT and DCH, and by an internally reflecting ring imaging Cherenkov detector. Muons are identified in the solenoid's instrumented flux return.

The events of the process under study and the background processes $e^+e^- \to \pi^+\pi^-\gamma$, $K^+K^-\gamma$, and $\mu^+\mu^-\gamma$ are simulated with the PHOKHARA [7] event generator, which takes into account next-to-leading-order radiative corrections. To estimate the model uncertainty of our measurement, the simulation for the signal process is performed under two form-factor assumptions, namely $|G_M| = |G_E|$ and $|G_E| = 0$. To obtain realistic estimates of pion and kaon backgrounds, the experimental values of the pion and kaon electromagnetic form factors measured by the CLEO Collaboration at $\sqrt{s} = 3.67$ GeV [10] are used in the event generator. The invariant-mass

[1]Throughout this paper, the asterisk denotes quantities in the e^+e^- c.m. frame; all other variables are given in the laboratory frame.

dependence of the form factors is assumed to be $1/m^2$, according to the QCD prediction for the asymptotic behavior of the form factors [17]. The $e^+e^- \to e^+e^-\gamma$ process is simulated with the BHWIDE [18] event generator.

The background from the two-photon process $e^+e^- \to e^+e^-p\bar{p}$ is simulated with the GamGam event generator [19]. In addition, possible background contributions from $e^+e^- \to q\bar{q}$, where q represents an u, d or s quark, are simulated with the JETSET [20] event generator. Since JETSET also generates ISR events, it can be used to study the background from ISR processes with extra π^0's, such as $e^+e^- \to p\bar{p}\pi^0\gamma$, $p\bar{p}\pi^0\pi^0\gamma$, etc. The most important non-ISR background process, $e^+e^- \to p\bar{p}\pi^0$, is simulated separately [1].

The detector response is simulated using the GEANT4 [21] package. The simulation takes into account the variations in the detector and beam background conditions over the running period of the experiment.

III. EVENT SELECTION

We select events with two charged particle tracks with opposite charges originating from the interaction region. Each track must have a transverse momentum greater than 0.1 GeV/c, be in the polar angle range $25.8° < \theta < 137.5°$, and be identified as a proton or antiproton. The pair of proton and antiproton candidates is fit to a common vertex with a beam-spot constraint, and the χ^2 probability for this fit is required to exceed 0.1%.

The final event selection is based on two variables: the $p\bar{p}$ transverse momentum (p_T) and the missing mass squared ($M^2_{\rm miss}$) recoiling against the $p\bar{p}$ system. The p_T distribution for simulated $e^+e^- \to p\bar{p}\gamma$ events is shown in Fig. 2. The peak near zero corresponds to ISR photons emitted along the collision axis, while the long tail is due to photons emitted at large angles. We apply the condition $p_T < 0.15$ GeV/c, which removes large-angle ISR events and strongly suppresses the background from the process $e^+e^- \to p\bar{p}\pi^0$ and from ISR processes with extra π^0's. The process $e^+e^- \to p\bar{p}\pi^0$ was the dominant background source at large invariant masses in our previous studies of the $e^+e^- \to p\bar{p}\gamma$ process with large-angle ISR [1,2].

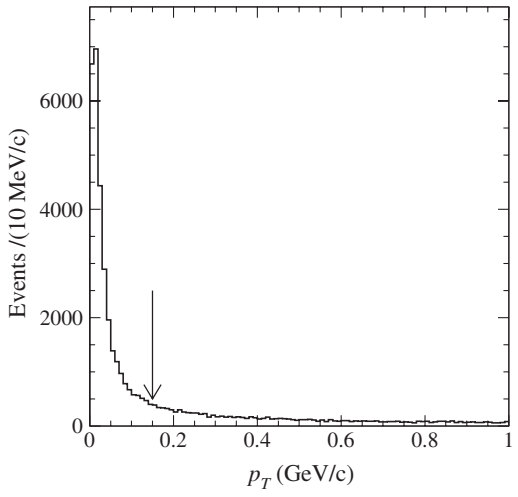

FIG. 2. The distribution of the $p\bar{p}$ transverse momentum for simulated $e^+e^- \to p\bar{p}\gamma$ events. The arrow indicates $p_T = 0.150$ GeV/c.

In the e^+e^- c.m. frame, protons with low $p\bar{p}$ invariant masses are produced in a narrow cone around the vector opposite to the ISR photon direction. Due to limited detector acceptance, the low-mass region cannot be studied with small-angle ISR. A $p\bar{p}$ pair with $p_T < 0.15$ GeV/c is detected in *BABAR* when its invariant mass is larger than 3.0 (4.5) GeV/c^2 for an ISR photon emitted along the electron (positron) beam direction. The corresponding average proton or antiproton momentum in the laboratory frame is about 2 (5) GeV/c. The difference between the two photon directions arises from the energy asymmetry of the e^+e^- collisions at PEP-II. Since particle misidentification probability strongly increases at large momentum, we reject events with the ISR photon emitted along the positron beam. This condition decreases the detection efficiency by about 20% for signal events with invariant masses above 5 GeV/c^2.

The missing-mass-squared distribution for simulated $e^+e^- \to p\bar{p}\gamma$ events is shown in Fig. 3. We select events with $|M^2_{\rm miss}| < 1$ GeV$^2/c^4$. This condition suppresses the background from two-photon and ISR events, which have large positive $M^2_{\rm miss}$, and the background from $e^+e^- \to e^+e^-\gamma$, $\mu^+\mu^-\gamma$ events, which have negative $M^2_{\rm miss}$. The sideband regions in $M^2_{\rm miss}$ and in p_T for ISR backgrounds are used to estimate the remaining background contributions from these sources.

The $p\bar{p}$ invariant-mass spectrum for the selected data candidates is shown in Fig. 4. The total number of selected events is 845. About 80% of the selected events originate

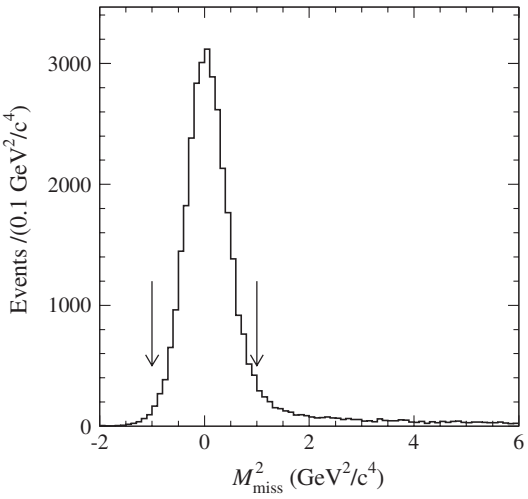

FIG. 3. The $M^2_{\rm miss}$ distribution for simulated $e^+e^- \to p\bar{p}\gamma$ events, where $M^2_{\rm miss}$ is the missing mass squared recoiling against the $p\bar{p}$ system. The arrows indicate $|M^2_{\rm miss}| = 1$ GeV$^2/c^4$.

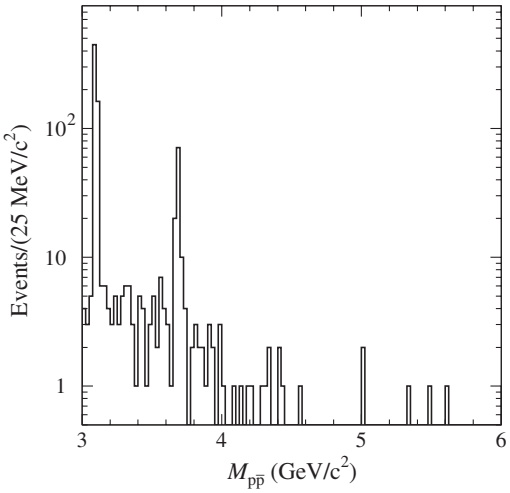

FIG. 4. The $p\bar{p}$ invariant-mass spectrum for selected data $p\bar{p}\gamma$ candidates.

from $J/\psi \to p\bar{p}$ and $\psi(2S) \to p\bar{p}$ decays. We do not observe events with invariant mass above 6 GeV$/c^2$.

IV. BACKGROUND ESTIMATION AND SUBTRACTION

The processes $e^+e^- \to \pi^+\pi^-\gamma$, $K^+K^-\gamma$, $\mu^+\mu^-\gamma$, and $e^+e^-\gamma$, in which the charged particles are misidentified as protons, are potential sources of background in the sample of selected data events. In addition, the two-photon process $e^+e^- \to e^+e^-p\bar{p}$ and processes with protons and neutral particles in the final state, such as $e^+e^- \to p\bar{p}\pi^0$ and $e^+e^- \to p\bar{p}\pi^0\gamma$, may yield background contributions.

A. Background from $e^+e^- \to \pi^+\pi^-\gamma$, $e^+e^- \to K^+K^-\gamma$, $e^+e^- \to \mu^+\mu^-\gamma$, and $e^+e^- \to e^+e^-\gamma$

In Ref. [2] it was shown that the *BABAR* MC simulation reproduces reasonably well the probability for a pion or a kaon to be identified as a proton. Consequently, the simulation is used to estimate the $e^+e^- \to \pi^+\pi^-\gamma$ and $e^+e^- \to K^+K^-\gamma$ background contributions in the present analysis. No events satisfying the selection criteria for $p\bar{p}\gamma$ are observed in the $\pi^+\pi^-\gamma$ and $K^+K^-\gamma$ MC samples. Since the sizes of these MC samples exceed those expected for pion and kaon events in data by about an order of magnitude, we conclude that these background sources can be neglected.

To estimate the possible electron and muon background, a method based on the difference in the $M^2_{\rm miss}$ distributions for signal and background events is used. For $e^+e^- \to \mu^+\mu^-\gamma$ events, the ratio of the number of events with $|M^2_{\rm miss}| < 1$ GeV$^2/c^4$ to the number with $M^2_{\rm miss} < -1$ GeV$^2/c^4$ varies from 0.03 to about 0.1 in the $M_{p\bar{p}}$ range of interest. Smaller values are expected for $e^+e^- \to e^+e^-\gamma$ events. In data we observe 15 events with $M^2_{\rm miss} < -1$ GeV$^2/c^4$, of which six events are expected to originate from the signal [of these, five are from $J/\psi \to p\bar{p}$ and $\psi(2S) \to p\bar{p}$ decays]. From the ratio values given above, we estimate that the muon and electron background in our selected event sample does not exceed 1 event. The estimated background contributions for different invariant-mass intervals are listed in Table I.

TABLE I. The number of selected $p\bar{p}\gamma$ candidates ($N_{\rm data}$) and the estimated numbers of background events from the processes $e^+e^- \to \mu^+\mu^-\gamma$ and $e^+e^- \to e^+e^-\gamma$ ($N_{\ell\ell\gamma}$), $e^+e^- \to e^+e^-p\bar{p}$ ($N_{2\gamma}$), and the ISR processes with extra neutral particle(s), such as $e^+e^- \to p\bar{p}\pi^0\gamma$, $p\bar{p}2\pi^0\gamma$ ($N^{\rm ISR}_{\rm bkg}$). In the invariant-mass intervals 3.0–3.2 GeV$/c^2$ and 3.6–3.8 GeV$/c^2$, the contributions of the $J/\psi \to p\bar{p}$ and $\psi(2S) \to p\bar{p}$ decays are subtracted (see Sec. VI), with related statistical uncertainties reported.

$M_{p\bar{p}}$ (GeV$/c^2$)	$N_{\rm data}$	$N_{\ell\ell\gamma}$	$N_{2\gamma}$	$N^{\rm ISR}_{\rm bkg}$
3.0–3.2	35 ± 7	<0.1	0.5 ± 0.4	1.5 ± 0.6
3.2–3.4	32	<0.1	0.5 ± 0.3	1.3 ± 0.6
3.4–3.6	31	<0.1	0.15 ± 0.10	0.7 ± 0.5
3.6–3.8	17 ± 5	<0.1	0.20 ± 0.10	0.0 ± 0.2
3.8–4.0	16	<0.1	0.10 ± 0.04	0.7 ± 0.4
4.0–4.5	12	<0.1	0.10 ± 0.03	0.7 ± 0.4
4.5–5.5	5	<0.3	0.05 ± 0.02	1.0 ± 0.5
5.5–6.5	1	<0.3	<0.01	0.4 ± 0.3

B. Two-photon background

Figure 5 shows the $M^2_{\rm miss}$ distribution for data events selected using all the criteria described in Sec. III except $|M^2_{\rm miss}| < 1$ GeV$^2/c^4$. Events with large recoil mass arise from the two-photon process $e^+e^- \to e^+e^-\gamma^*\gamma^* \to e^+e^-p\bar{p}$. The two-photon background in the region

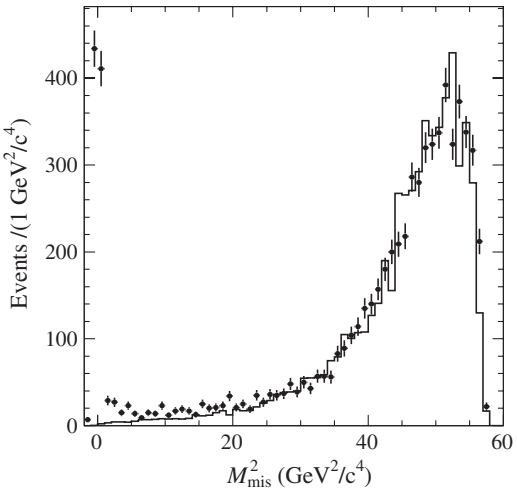

FIG. 5. The $M^2_{\rm miss}$ distribution for data events (points with error bars) selected using all the criteria described in Sec. III except $|M^2_{\rm miss}| < 1$ GeV$^2/c^4$. The solid histogram represents the distribution for simulated $e^+e^- \to e^+e^-p\bar{p}$ events. The simulated distribution is normalized to the number of data events with $M^2_{\rm miss} > 30$ GeV$^2/c^4$.

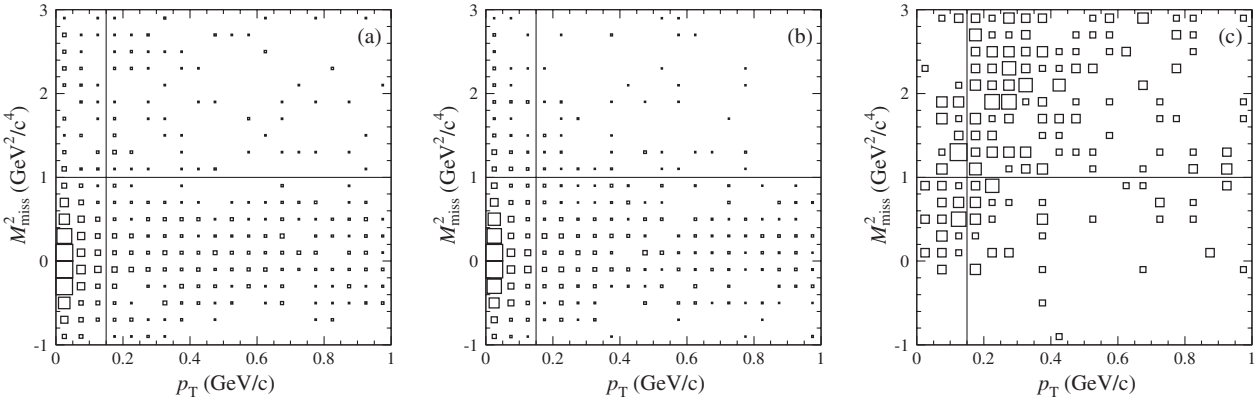

FIG. 6. The distributions of $M^2_{\rm miss}$ versus p_T (a) for data events with $M_{p\bar{p}} > 3.2$ GeV$/c^2$, (b) for simulated signal events, and (c) for simulated ISR background events.

$|M^2_{\rm miss}| < 1$ GeV$^2/c^4$ is estimated from the number of data events with $M^2_{\rm miss} > d$ using the scale factor $R_{\gamma\gamma} = N_{\gamma\gamma}(|M^2_{\rm miss}| < 1)/N_{\gamma\gamma}(M^2_{\rm miss} > d)$ obtained from the $e^+e^- \to e^+e^- p\bar{p}$ simulation. Since the $M^2_{\rm miss}$ distribution for two-photon events changes with $p\bar{p}$ invariant mass, the parameter d is changed from 40 GeV$^2/c^4$ for the invariant-mass interval 3.0–3.2 GeV$/c^2$ to 15 GeV$^2/c^4$ for the interval 5.5–6.5 GeV$/c^2$. To determine a realistic value of the scale factor, the simulated events are reweighted according to the proton angular distribution observed in data. The $M^2_{\rm miss}$ distribution for reweighted simulated events is shown in Fig. 5 in comparison with the data distribution. The value of the scale factor is found to increase from 5×10^{-4} in the 3.0–3.2 GeV$/c^2$ interval to 2×10^{-2} in the 5.5–6.5 GeV$/c^2$ interval. Fortunately, the number of observed two-photon events decreases significantly over this same range. The estimated number of two-photon background events for each invariant-mass interval is listed in Table I. The uncertainty on the number of background events is determined by statistics of MC simulation and the non-$\gamma\gamma \to p\bar{p}$ background at large $M_{p\bar{p}}$. The background is found to be small, at the level of 1%.

C. ISR background

To estimate the background from ISR processes with at least one extra neutral particle, such as $e^+e^- \to p\bar{p}\pi^0\gamma$, $e^+e^- \to p\bar{p}\eta\gamma$, $e^+e^- \to p\bar{p}\pi^0\pi^0\gamma$, etc., we use differences in the p_T and $M^2_{\rm miss}$ distributions for signal and background events. Figure 6 shows the two-dimensional distributions of $M^2_{\rm miss}$ versus p_T for data events with $M_{p\bar{p}} > 3.2$ GeV$/c^2$, and for simulated signal and ISR background events. The ISR background is simulated using the JETSET event generator. It should be noted that most of the background events (about 90%) shown in Fig. 6 arise from $e^+e^- \to p\bar{p}\pi^0\gamma$. The lines in Fig. 6 indicate the boundaries of the signal region (bottom-left rectangle) and of the sideband region (top-right rectangle). The number of data events in the sideband (N_2) is used to estimate the number of background events in the signal region by using

$$N^{\rm ISR}_{\rm bkg} = \frac{N_2 - \beta_{\rm sig} N_1}{\beta_{\rm bkg} - \beta_{\rm sig}}, \tag{4}$$

where N_1 is the number of data events in the signal region, and $\beta_{\rm sig}$ and $\beta_{\rm bkg}$ are the N_2/N_1 ratios for the signal and background, respectively. These ratios are determined from MC simulation to be $\beta_{\rm sig} = 0.043 \pm 0.002$ and $\beta_{\rm bkg} = 5 \pm 1$. Both coefficients are found to be practically independent of $p\bar{p}$ invariant mass. The estimated numbers of ISR background events for different invariant-mass regions are listed in Table I. This is the main source of background for the process under study.

The background from the process $e^+e^- \to p\bar{p}\pi^0$, which was the dominant background source in our previous large-angle studies [1,2], is found to be negligible in the data sample selected with the criteria for small-angle ISR events.

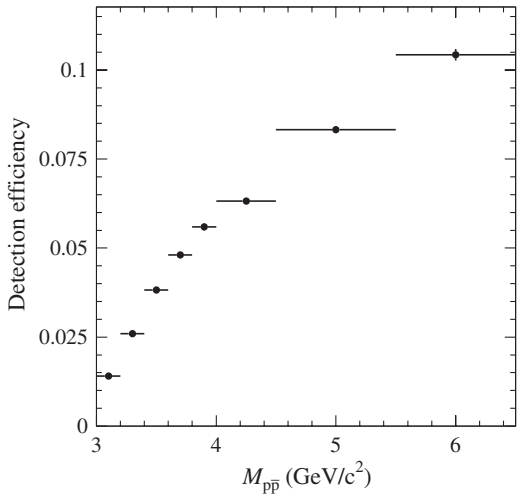

FIG. 7. The $p\bar{p}$ invariant-mass dependence of the detection efficiency obtained from MC simulation in the model with $|G_E| = |G_M|$.

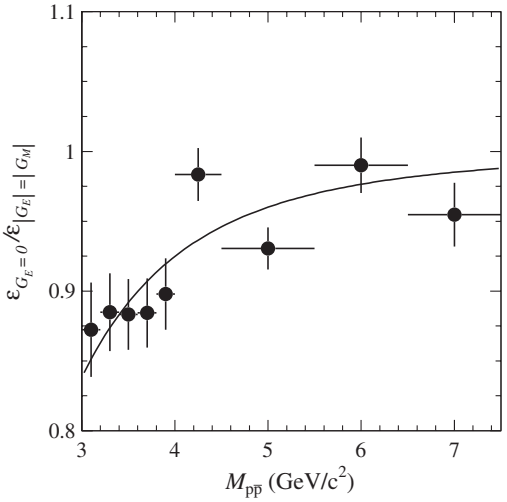

FIG. 8. The ratio of the detection efficiencies obtained from MC simulation using $G_E = 0$ and using $|G_E| = |G_M|$. The solid curve is drawn to guide the eye.

V. DETECTION EFFICIENCY

The detection efficiency determined using MC simulation is shown in Fig. 7 as a function of $p\bar{p}$ invariant mass. The efficiency is calculated under the assumption that $|G_E| = |G_M|$. To study the model dependence of the detection efficiency, we analyze a sample of MC events produced using a model with $G_E = 0$. The ratio of the efficiencies obtained in the two models is shown in Fig 8. The deviation of this ratio from unity is taken as an estimate of the model uncertainty on the detection efficiency.

The efficiency determined from MC simulation ($\varepsilon_{\rm MC}$) must be corrected to account for data-MC simulation differences in detector response according to

$$\varepsilon = \varepsilon_{\rm MC} \prod (1 + \delta_i), \tag{5}$$

where the δ_i are the efficiency corrections listed in Table II. The corrections for data-MC simulation differences in track reconstruction, nuclear interaction, and PID were estimated in our previous publications [1,2]. Systematic effects on p_T and $M^2_{\rm miss}$ may bias the estimated efficiency through the selection criteria. This is studied using $e^+e^- \to J/\psi\gamma \to p\bar{p}\gamma$ events. In Sec. VI, the number of J/ψ events is determined with the requirements $p_T < 1$ GeV/c and $-2 < M^2_{\rm miss} < 3$ GeV$^2/c^4$, which are significantly looser than our standard criteria. The double data-MC simulation ratio of the numbers of J/ψ events selected with the standard and looser criteria, 1.043 ± 0.026, is used to estimate the efficiency correction. The corrected values of the detection efficiency are listed in Table III.

TABLE II. The values of the efficiency corrections, δ_i.

Source	δ_i (%)
Track reconstruction	0.0 ± 0.5
Nuclear interaction	1.1 ± 0.4
PID	-1.9 ± 2.0
Conditions on p_T and $M^2_{\rm miss}$	4.3 ± 2.6
Total	3.5 ± 3.3

VI. J/ψ AND $\psi(2S)$ DECAYS INTO $p\bar{p}$

The $p\bar{p}$ invariant-mass spectra for selected events in the J/ψ and $\psi(2S)$ invariant-mass regions are shown in Fig. 9. The events are selected by requiring $p_T < 1$ GeV/c and $-2 < M^2_{\rm miss} < 3$ GeV$^2/c^4$. To determine the number of resonance events, both spectra are fitted using the sum of a probability density function (PDF) for resonance events and a linear background function. The resonance PDF is a Breit-Wigner function convolved with a double Gaussian function describing detector resolution. The parameters of the resolution function are determined from simulation.

TABLE III. The $p\bar{p}$ invariant-mass interval ($M_{p\bar{p}}$), number of selected events (N) after background subtraction, detection efficiency (ε), ISR luminosity (L), measured $e^+e^- \to p\bar{p}$ cross section ($\sigma_{p\bar{p}}$), and proton magnetic form factor ($|G_M|$). The quoted uncertainties are statistical. The systematic uncertainty is 4% for the cross section and 2% for the form factor. The model uncertainty for the cross section (form factor) is 15 (8)% at 3 GeV, decreases to 5 (3)% at 4.5 GeV, and does not exceed 5 (3)% at higher values.

$M_{p\bar{p}}$ (GeV/c^2)	N	ε (%)	L (pb^{-1})	$\sigma_{p\bar{p}}$ (pb)	$\lvert G_M\rvert$
3.0–3.2	33.0 ± 7.0	1.45	271	8.4 ± 1.8	$0.0310^{+0.0031}_{-0.0035}$
3.2–3.4	30.0 ± 5.7	2.69	292	3.8 ± 0.7	$0.0221^{+0.0020}_{-0.0022}$
3.4–3.6	30.0 ± 5.6	3.95	314	2.42 ± 0.45	$0.0186^{+0.0017}_{-0.0018}$
3.6–3.8	16.4 ± 5.1	4.97	337	0.98 ± 0.30	$0.0124^{+0.0018}_{-0.0021}$
3.8–4.0	15.0 ± 4.0	5.79	361	0.72 ± 0.19	$0.0112^{+0.0014}_{-0.0016}$
4.0–4.5	11.0 ± 3.5	6.54	1018	0.165 ± 0.053	$0.0058^{+0.0009}_{-0.0010}$
4.5–5.5	4.0 ± 2.3	8.62	2637	0.018 ± 0.010	$0.0022^{+0.0006}_{-0.0008}$
5.5–6.5	0.6 ± 1.1	10.79	4079	0.0014 ± 0.0025	$0.0007^{+0.0005}_{-0.0007}$

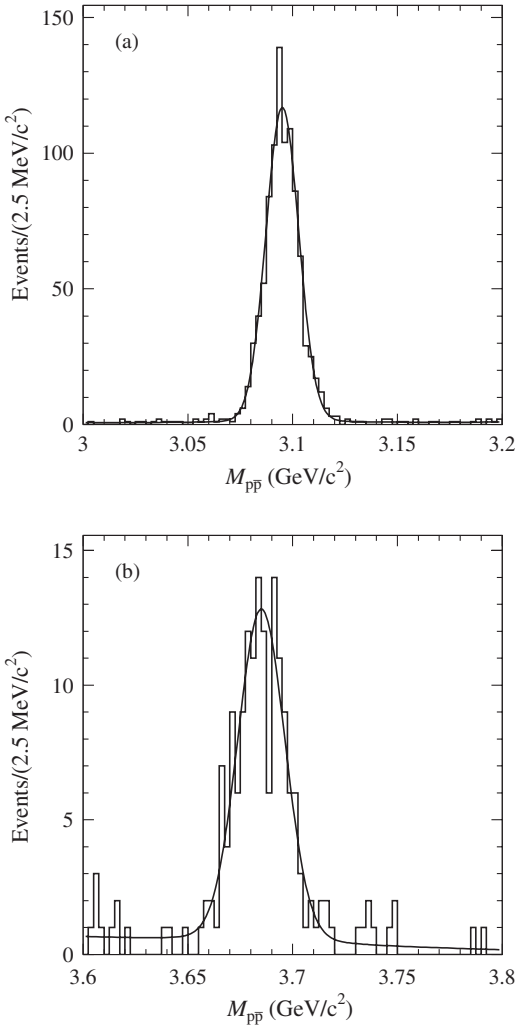

FIG. 9. The $p\bar{p}$ invariant-mass spectrum in the invariant-mass region near (a) the J/ψ, and (b) the $\psi(2S)$. The curves show the results of the fits described in the text.

To account for possible differences in detector response between data and simulation, the simulated resolution function is modified by allowing an additional σ_G to be added in quadrature to both σ's of the double Gaussian function and by introducing the possibility of an invariant-mass shift. The free parameters in the fit to the J/ψ invariant-mass region are the number of resonance events, the total number of nonresonant background events, the slope of the background function, σ_G, and the mass-shift parameter. In the $\psi(2S)$ fit, σ_G is fixed to the value obtained from the J/ψ fit. The result of the fit for the J/ψ region is shown by the solid curve in Fig. 9(a), and the corresponding signal yield is 918 ± 31 events. Similarly, the solid curve in Fig. 9(b) shows the fit result for the $\psi(2S)$ region, with the signal yield of 142 ± 13 events. The other fit parameters are $\sigma_G = 1.4 \pm 0.8\,\mathrm{MeV}$, $M_{J/\psi} - M^{\mathrm{MC}}_{J/\psi} = -0.5 \pm 0.3\,\mathrm{MeV}/c^2$, $M_{\psi(2S)} - M^{\mathrm{MC}}_{\psi(2S)} = -0.9 \pm 1.0\ \mathrm{MeV}/c^2$. The fitted value of σ_G corresponds to a 1.5% difference in the mass resolution (about 8 MeV at J/ψ) between data and simulation.

The detection efficiency is estimated from MC simulation. The event generator uses the experimental data on the polar-angle distribution of the proton in $\psi \to p\bar{p}$ decay. The distribution is described by the function $1 + a\cos^2\vartheta$ with $a = 0.595 \pm 0.019$ for J/ψ [22] and 0.72 ± 0.13 for $\psi(2S)$ [23,24]. The model error on the detection efficiency due to the uncertainty of a is estimated to be 1.5% for the J/ψ and 5% for the $\psi(2S)$. The efficiencies ($\varepsilon_{\mathrm{MC}}$) are found to be $(2.20 \pm 0.02)\%$ for the J/ψ and $(6.86 \pm 0.04)\%$ for the $\psi(2S)$. The data-MC simulation differences discussed earlier are used to correct the above efficiency values by $(-0.8 \pm 2.1)\%$ (Table II, corrections 1–3).

The value of the cross section for the production of the J/ψ or $\psi(2S)$ followed by its decay to $p\bar{p}$ is given by $N/(\varepsilon L)$, where N is the number of signal events extracted in the fit shown in Figs. 9(a) or 9(b), ε is the relevant detection efficiency, and L is the nominal integrated luminosity. The cross section values obtained in this way are $(89.5 \pm 3.0 \pm 2.8)$ fb and $(4.45 \pm 0.41 \pm 0.25)$ fb for the J/ψ and $\psi(2S)$, respectively, where the first error is statistical and the second systematic.

These values correspond to the integral of the right-hand side of Eq. (1) over the resonance lineshape, i.e. for resonance R,

$$\sigma_{\mathrm{meas}} = \int \frac{2m}{s} W(s,x)\sigma_R(m)\mathrm{d}m, \tag{6}$$

where m runs over the resonance region. For a narrow resonance,

$$\sigma_{\mathrm{meas}} = W(s,x_R)\frac{12\pi^2}{s}\frac{\Gamma(R \to e^+e^-)\mathcal{B}(R \to p\bar{p})}{m_R} \tag{7}$$

is a very good approximation, where $x_R = 1 - m_R^2/s$, and m_R is the resonance mass.

From the measured values of the cross section, we thus obtain

$$\begin{aligned}&\Gamma(J/\psi \to e^+e^-)\mathcal{B}(J/\psi \to p\bar{p})\\ &\quad = (12.9 \pm 0.4 \pm 0.4)\ \mathrm{eV},\\ &\Gamma(\psi(2S) \to e^+e^-)\mathcal{B}(\psi(2S) \to p\bar{p})\\ &\quad = (0.74 \pm 0.07 \pm 0.04)\ \mathrm{eV}.\end{aligned} \tag{8}$$

The systematic error includes the uncertainties of the detection efficiency, the integrated luminosity (1%), and the theoretical uncertainty on the production cross section (1%).

Using the nominal values of the e^+e^- widths [25], the $\psi \to p\bar{p}$ branching fractions are calculated to be

$$\begin{aligned}\mathcal{B}(J/\psi \to p\bar{p}) &= (2.33 \pm 0.08 \pm 0.09) \times 10^{-3},\\ \mathcal{B}(\psi(2S) \to p\bar{p}) &= (3.14 \pm 0.28 \pm 0.18) \times 10^{-4}.\end{aligned} \tag{9}$$

These values are in agreement with the corresponding nominal values [25], $(2.17 \pm 0.07) \times 10^{-3}$ and $(2.76 \pm 0.12) \times 10^{-4}$, and with the recent BESIII measurement [22] $\mathcal{B}(J/\psi \to p\bar{p}) = (2.11 \pm 0.03) \times 10^{-3}$.

VII. THE $e^+e^- \to p\bar{p}$ CROSS SECTION AND THE PROTON FORM FACTOR

The cross section for $e^+e^- \to p\bar{p}$ in each $p\bar{p}$ invariant-mass interval i is calculated as $N_i/(\varepsilon_i L_i)$. The number of selected events (N_i) for each $p\bar{p}$ invariant-mass interval after background subtraction is listed in Table III. The values of the L_i (Table III) have been obtained by integration of $W(s, x)$ from Refs. [4,5] over each invariant-mass interval. They can also be calculated using the PHOKHARA event generator [7]. The results of the two calculations agree within 0.5%, which coincides with the estimated theoretical accuracy of the PHOKHARA generator [7]. The obtained values of the $e^+e^- \to p\bar{p}$ cross section are listed in Table III. For the invariant-mass intervals 3.0–3.2 GeV/c^2 and 3.6–3.8 GeV/c^2, we quote the nonresonant cross sections with the respective J/ψ and $\psi(2S)$ contributions excluded. The quoted errors are statistical, as obtained from the uncertainty in the number of selected $p\bar{p}\gamma$ events. The systematic uncertainty is independent of invariant mass and is equal to 4%. It includes the statistical error of the detection efficiency (2%), the uncertainty of the efficiency correction (3.3%), the uncertainty in the integrated luminosity (1%), and an uncertainty in the ISR luminosity (0.5%). The model uncertainty due to the unknown $|G_E/G_M|$ ratio (see Fig. 8) is about 15% at 3 GeV/c^2, decreases to 5% at 4.5 GeV/c^2, and does not exceed 5% at higher values. The measured $e^+e^- \to p\bar{p}$ cross section is shown in Fig. 10 together with the results of previous e^+e^- measurements.

The values of the proton magnetic form factor are obtained using Eq. (3) under the assumption that $|G_E| = |G_M|$. They are listed in Table III and shown in Fig. 11 (linear scale) and in Fig. 12 (logarithmic scale). It is seen that our results are in good agreement with the results from other experiments. The curve in Fig. 12 is the result of a fit of the asymptotic QCD dependence of the proton form factor [14], $|G_M| \sim \alpha_s^2(M_{p\bar{p}}^2)/M_{p\bar{p}}^4 \sim D/(M_{p\bar{p}}^4 \log^2(M_{p\bar{p}}^2/\Lambda^2))$, to all the existing data with $M_{p\bar{p}} > 3$ GeV/c^2, excluding the two points from Ref. [11]. Here $\Lambda = 0.3$ GeV, and D is a free fit parameter. The data are well described by this function, with $\chi^2/\nu = 17/24$, where ν is the number of degrees of freedom. Including the points from Ref. [11] in the fit increases χ^2/ν to 54/26.

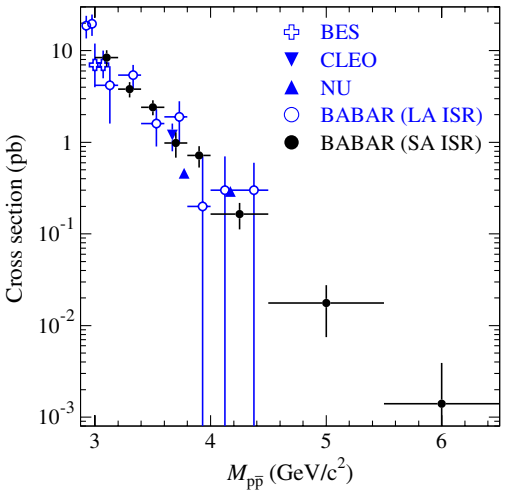

FIG. 10 (color online). The $e^+e^- \to p\bar{p}$ cross section measured in this analysis [*BABAR* (SA ISR)] and in other experiments: BES [9], CLEO [10], NU [11], and *BABAR* (LA ISR) [2].

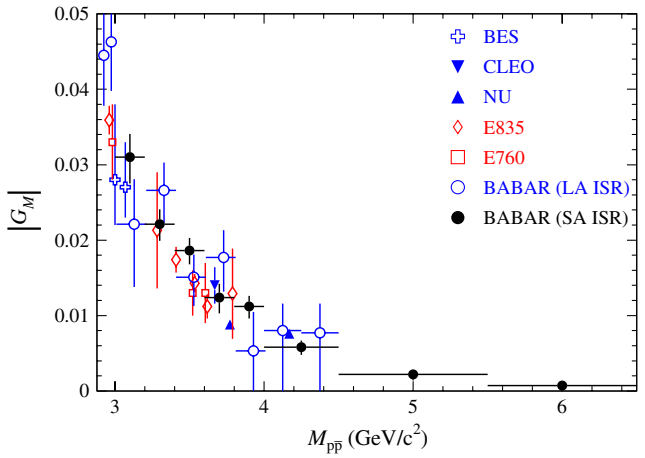

FIG. 11 (color online). The proton magnetic form factor measured in this analysis [*BABAR* (SA ISR)] and in other experiments: BES [9], CLEO [10], NU [11], E835 [13], E760 [12], *BABAR* (LA ISR) [2].

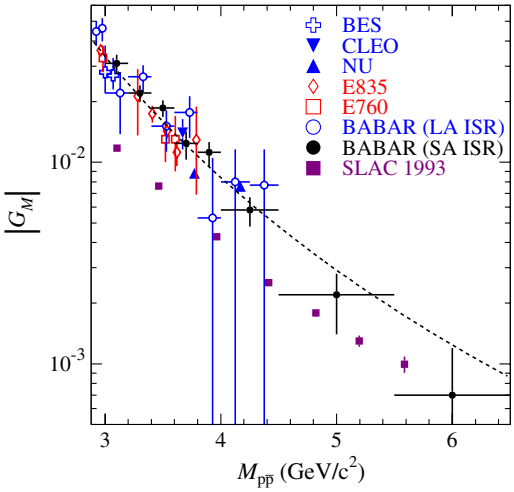

FIG. 12 (color online). The proton magnetic form factor measured in this analysis [*BABAR* (SA ISR)] and in other experiments: BES [9], CLEO [10], NU [11], E835 [13], E760 [12], *BABAR* (LA ISR) [2]. Points denoted by "SLAC 1993" represent data on the spacelike magnetic form factor obtained in ep scattering [26] as a function of $\sqrt{-q^2}$, where q^2 is the momentum transfer squared. The curve is the result of the QCD-motivated fit described in the text.

In Fig. 12, we also show the spacelike $|G_M|$ data ("SLAC 1993" points) obtained in Ref. [26]. The QCD prediction is that the space- and timelike asymptotic values will be the same. In the region from 3.0 to 4.5 GeV/c^2, the value of the timelike form factor is about 2 times larger than that of the spacelike one. Our points above 4.5 GeV/c^2 give some indication that the difference between time- and spacelike form factors may be decreasing, although our measurement uncertainties are large in this region.

VIII. SUMMARY

The process $e^+e^- \to p\bar{p}\gamma$ has been studied in the $p\bar{p}$ invariant-mass range from 3.0 to 6.5 GeV/c^2 for events with an undetected ISR photon emitted close to the collision axis. From the measured $p\bar{p}$ invariant-mass spectrum we extract the $e^+e^- \to p\bar{p}$ cross section and determine the magnitude of the magnetic form factor of the proton. This is the first measurement of the proton form factor at $p\bar{p}$ invariant masses higher than 4.5 GeV/c^2. The observed strong decrease of the form factor agrees with the asymptotic dependence $\alpha_s^2(M_{p\bar{p}}^2)/M_{p\bar{p}}^4$ predicted by QCD.

The branching fractions for the decays $J/\psi \to p\bar{p}$ and $\psi(2S) \to p\bar{p}$ have been measured, and the values

$$\begin{aligned}\mathcal{B}(J/\psi \to p\bar{p}) &= (2.33 \pm 0.08 \pm 0.09) \times 10^{-3},\\ \mathcal{B}(\psi(2S) \to p\bar{p}) &= (3.14 \pm 0.28 \pm 0.18) \times 10^{-4}\end{aligned} \tag{10}$$

have been obtained. These values are in agreement with previous measurements.

ACKNOWLEDGMENTS

We are grateful for the extraordinary contributions of our PEP-II colleagues in achieving the excellent luminosity and machine conditions that have made this work possible. The success of this project also relies critically on the expertise and dedication of the computing organizations that support *BABAR*. The collaborating institutions wish to thank SLAC for its support and the kind hospitality extended to them. This work is supported by the U.S. Department of Energy and National Science Foundation, the Natural Sciences and Engineering Research Council (Canada), the Commissariat à l'Energie Atomique and Institut National de Physique Nucléaire et de Physique des Particules (France), the Bundesministerium für Bildung und Forschung and Deutsche Forschungsgemeinschaft (Germany), the Istituto Nazionale di Fisica Nucleare (Italy), the Foundation for Fundamental Research on Matter (Netherlands), the Research Council of Norway, the Ministry of Education and Science of the Russian Federation, Ministerio de Ciencia e Innovación (Spain), and the Science and Technology Facilities Council (United Kingdom). Individuals have received support from the Marie-Curie IEF program (European Union) and the A. P. Sloan Foundation (U.S.).

[1] B. Aubert *et al.* (*BABAR* Collaboration), Phys. Rev. D **73**, 012005 (2006).
[2] J. P. Lees *et al.* (*BABAR* Collaboration), Phys. Rev. D **87**, 092005 (2013).
[3] V. P. Druzhinin, S. I. Eidelman, S. I. Serednyakov, and E. P. Solodov, Rev. Mod. Phys. **83**, 1545 (2011).
[4] O. Nicrosini and L. Trentadue, Phys. Lett. B **196**, 551 (1987).
[5] F. A. Berends, W. L. van Neerven, and G. J. H. Burgers, Nucl. Phys. **B297**, 429 (1988); **B304**, 712 (1988).
[6] M. Benayoun, S. I. Eidelman, V. N. Ivanchenko, and Z. K. Silagadze, Mod. Phys. Lett. A **14**, 2605 (1999).
[7] H. Czyz, A. Grzelinska, J. H. Kuhn, and G. Rodrigo, Eur. Phys. J. C **39**, 411 (2005).
[8] A. B. Arbuzov and T. V. Kopylova, J. High Energy Phys. 04 (2012) 009.
[9] M. Ablikim *et al.* (BES Collaboration), Phys. Lett. B **630**, 14 (2005).
[10] T. K. Pedlar *et al.* (CLEO Collaboration), Phys. Rev. Lett. **95**, 261803 (2005).
[11] K. K. Seth, S. Dobbs, Z. Metreveli, A. Tomaradze, T. Xiao, and G. Bonvicini, Phys. Rev. Lett. **110**, 022002 (2013).
[12] T. A. Armstrong *et al.* (E760 Collaboration), Phys. Rev. Lett. **70**, 1212 (1993).
[13] M. Ambrogiani *et al.* (E835 Collaboration), Phys. Rev. D **60**, 032002 (1999); M. Ambrogiani *et al.* (E835 Collaboration), Phys. Lett. B **559**, 20 (2003).
[14] V. L. Chernyak and A. R. Zhitnitsky, JETP Lett. **25**, 510 (1977); G. P. Lepage and S. J. Brodsky, Phys. Rev. Lett. **43**, 545 (1979).
[15] J. P. Lees *et al.* (*BABAR* Collaboration), Nucl. Instrum. Methods Phys. Res., Sect. A **726**, 203 (2013).
[16] B. Aubert *et al.* (*BABAR* Collaboration), Nucl. Instrum. Methods Phys. Res., Sect. A **479**, 1 (2002); B. Aubert *et al.* (*BABAR* Collaboration), Nucl. Instrum. Methods Phys. Res., Sect. A **729**, 615 (2013).
[17] V. L. Chernyak, A. R. Zhitnitsky, and V. G. Serbo, Pisma Zh. Eksp. Teor. Fiz. **26**, 760 (1977) [JETP Lett. **26**, 594 (1977)].
[18] S. Jadach, W. Placzek, and B. F. L. Ward, Phys. Lett. B **390**, 298 (1997).
[19] B. Aubert *et al.* (*BABAR* Collaboration), Phys. Rev. D **81**, 092003 (2010).
[20] T. Sjöstrand, Comput. Phys. Commun. **82**, 74 (1994).

[21] S. Agostinelli *et al.* (Geant4 Collaboration), Nucl. Instrum. Methods Phys. Res., Sect. A **506**, 250 (2003).
[22] M. Ablikim *et al.* (BESIII Collaboration), Phys. Rev. D **86**, 032014 (2012).
[23] M. Ambrogiani *et al.* (E835 Collaboration), Phys. Lett. B **610**, 177 (2005).
[24] M. Ablikim *et al.* (BES Collaboration), Phys. Lett. B **648**, 149 (2007).
[25] J. Beringer *et al.* (Particle Data Group), Phys. Rev. D **86**, 010001 (2012).
[26] A. F. Sill *et al.*, Phys. Rev. D **48**, 29 (1993).